HYPERVELOCITY IMPACT ON CARBON FIBRE REINFORCED PLASTIC (CFRP)/ALUMINIUM HONEYCOMB AT NORMAL AND OBLIQUE ANGLES

Emma A. Taylor[1], Mark K. Herbert[1/2] and Laurie Kay[1]

[1] *Unit for Space Sciences and Astrophysics, University of Kent at Canterbury, Canterbury, CT2 7NR, U.K.*
(phone: +44 1227 764000 xt 3834 fax: +44 1227 762616 email: eat1@ukc.ac.uk)
[2] *Matra Marconi Space (UK) Ltd, FPC 310, PO Box 16, Filton, Bristol, BS12 7YB, U.K.*

ABSTRACT

CFRP/Al-HC is in common use as a spacecraft structural material and provides good performance in terms of high strength, low weight and low thermal distortion. The response of this material to hypervelocity impact has been, until now, poorly characterised, although the channelling behaviour of the honeycomb has been known since at least 1970 (Ref. 1). Its increasing use, combined with the projected increase in the LEO debris population, requires better characterisation of its response to both normal and oblique hypervelocity impact. Recent work (Ref. 2) has shown the influence of projectile density on rear wall failure for normal impacts at 5 km s^{-1} and the production of five types of ejecta with the potential to affect spacecraft operations. We present results of oblique shots using 0.8-1.5 mm diameter aluminium, titanium and steel projectiles onto CFRP/Al-HC. The results from a previous impact programme (Ref. 2) onto CFRP/Al-HC are used to select the projectile diameters and densities in order to investigate the effect of angle of impact on the ballistic limit. X-ray testing of the normal and oblique impact targets from this and previous work (Ref. 2) is used to analyse the dependence of honeycomb cell damage on angle of impact. The total data set is used to continue the search for a CFRP/Al-HC damage equation. An assessment of the implications for subsystem design is provided.

SYMBOLS AND ABBREVIATIONS

A	area of hole (mm^2)
d	projectile diameter (mm)
D	diameter of impact feature (mm)
E	impact energy (J)
v	velocity (km s^{-1})
θ	impact angle (normal incidence, θ=0°)
ρ	density (g cm^{-3})
Al-HC	Aluminium facesheets + honeycomb
CFRP	Carbon Fibre Reinforced Plastic
EMC	ElectroMagnetic Compatibility
HC	honeycomb
HGF	hole growth factor HGF = ($D_{eq(rear)}/D_{eq(front)}$)
LEO	Low Earth Orbit
LGG	Light Gas Gun
MLI	Multi Layer Insulation
NDT	Non-Destructive Testing
PZT	Piezoelectric Transducer

Subscripts

a	along the direction of impact
b	perpendicular to the direction of impact
c	crater
eq	equivalent
front	impact feature on front of target
h	hole
p	projectile
rear	impact feature on rear of target
t	target

1. INTRODUCTION

This experimental programme investigates the damage mechanisms and morphology of a CFRP/Al-HC spacecraft structure near the ballistic limit[1], for oblique impacts, in the range 15-75° and at an impact velocity in the region of 5 km s^{-1}. The dependence of the damage on projectile diameter, density and impact angle is used to investigate whether a damage equation can be formulated. The body of work describing hypervelocity impact on composite materials is much smaller than that for metallic targets. We summarise selected previous work in Appendix 1, identifying results pertinent to the aims of this work.

2. EXPERIMENTAL PROGRAMME

The target material comprised CFRP facesheets with an aluminium honeycomb core, as typically used for a LEO space platform. The CFRP/Al-HC lay-up and material properties are given in Table 1. Details of the Light Gas Gun operations are described in Ref. 2. The projectiles used were spherical: nylon (ρ = 1.15 g cm^{-3}), cellulose acetate (1.45 g cm^{-3}), aluminium 2017 (2.78 g cm^{-3}), ruby (3.98 g cm^{-3}), titanium (4.54 g cm^{-3}), stainless steel AISI 420 (7.75 g cm^{-3}) and phosphor bronze (8.03 g cm^{-3}). The shot programme is given in Table 2. A total of 21 oblique shots are analysed, in addition to the data in Ref. 2 (13 normal incidence shots). X-ray analyses of the 34

[1] The ballistic limit is defined as marginal perforation of the rear surface of the target.

shots are also presented. The front and rear holes were digitally imaged and the projected area of the holes ($A_{h(front)}$ and $A_{h(rear)}$) were calculated via a pixel recognition/counting program and the appropriate scaling factor. By defining the hole damage A_h as an ellipse, the equivalent diameter (D_{eq}) was calculated using equation 1, excluding any delamination damage of the surface. Delamination damage is defined as material removed around the central hole which does not fully penetrate the surface. In addition, the hole diameter along the flight axis (D_a) and perpendicular to the flight axis (D_b) were measured. The elliptical ratio was calculated by taking the ratio (D_a/D_b).

$$D_{eq} = (4A_h / \pi)^{0.5} \qquad (1)$$

The internal honeycomb damage was measured using 30 keV X-rays. The exposed Polaroid film recorded the cell damage integrated over the target thickness. The resulting morphology was classified and the maximum damage area was determined using the same technique as for the CFRP hole. An estimate of the reproducibility of the shots was provided by analysis of two pairs of shots using identical projectiles, impact angles and velocities. The variation in the crater features was used to estimate the 'reproducibility' errors applied to the data.

Face sheets	
Prepreg matrix	4 ply satin woven carbon fibre epoxy HMF371-7714B
Fibre Orientation	0°/90°/90°/0°
Thickness	1.62 mm
Density	1800 - 1850 kg m^{-3}
Modulus of Elasticity	69.1 - 69.5 kN mm^{-2}
Honeycomb core	
Section type	Aeroweb
Material	Al Alloy 3003
Core density	83 kg m^{-3} (5.2 lb ft^{-3})
Cell size	6.4 mm (0.25 inches)
Cell foil thickness	0.06 mm (25 x 10^{-4} inches)
Core thickness	45 mm
Film adhesive	Redux 609 or 312

Table 1. Target material properties

Parameter	This work	Ref. 2
d_p (mm)	0.8, 1.0, 1.2, 1.5	0.8, 1.0, 1.2, 1.5, 2.0
v (km s^{-1})	4.8-5.8	4.5-6.2
ρ_p (g cm^{-3})	2.8-4.5	1.15 - 8.03
θ (°)	15, 25, 30, 45, 60, 75	0

Table 2. Shot programme details

3. RESULTS

3.1 Impact damage

The impact morphology of the composite facesheets and aluminium honeycomb can, in addition to determining the threshold for perforation, be used to assess ejecta production and future limitations on spacecraft performance. For both the normal and oblique shots, a large quantity of ejecta was produced from the rear target surface (classified in Ref. 2). In addition, loose material remained within the target (comprising metal and carbon fibre fragments) which were not retained during target handling.

3.2 Oblique impacts

The impact crater morphology progression is given in Fig. 1. The crater shape does not vary steadily with impact angle and the hole size increases with projectile density.

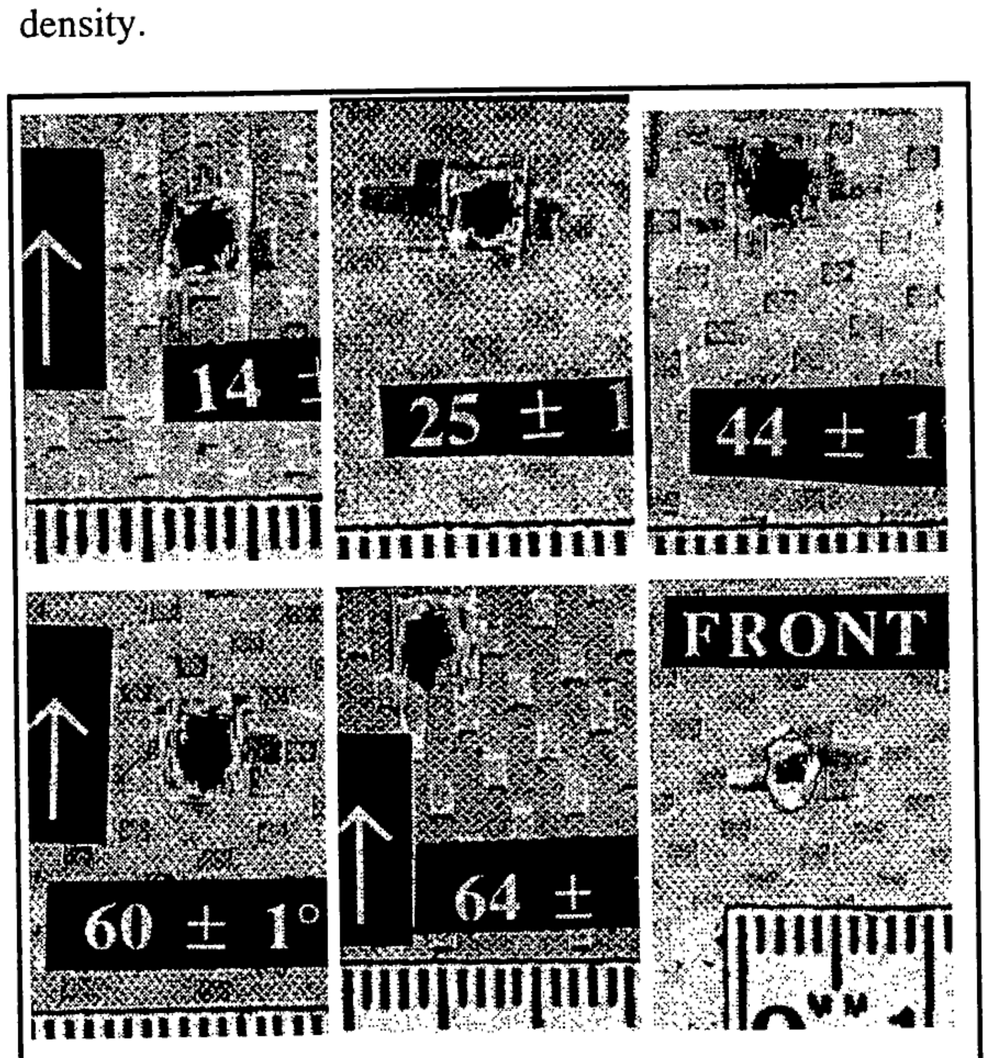

Figure 1. Crater morphology for impacts at a range of impact angles. The bottom right image is an impact at 75° and the outline shows the typical crater observed at this impact angle.

In Fig. 2, the ellipticity of the targets is plotted against the impact angle (measured from the normal). Impacts at angles greater than 45° show a clear ellipticity. In Fig. 3, D_a/d_p (the crater diameter along the line of flight, normalised by projectile diameter) is plotted against impact angle. There is a drop in D_a/d_p for low density projectiles at highly oblique impact angles, but not for the higher density projectiles.

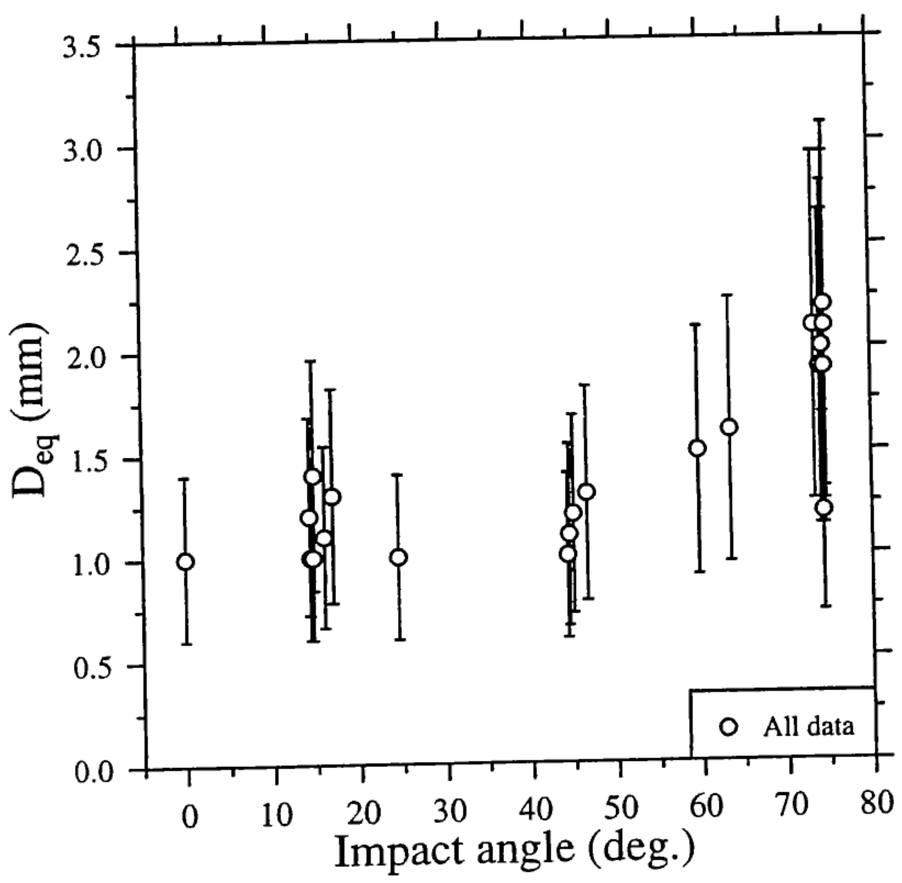

Figure 2. Ellipticity as a function of impact angle

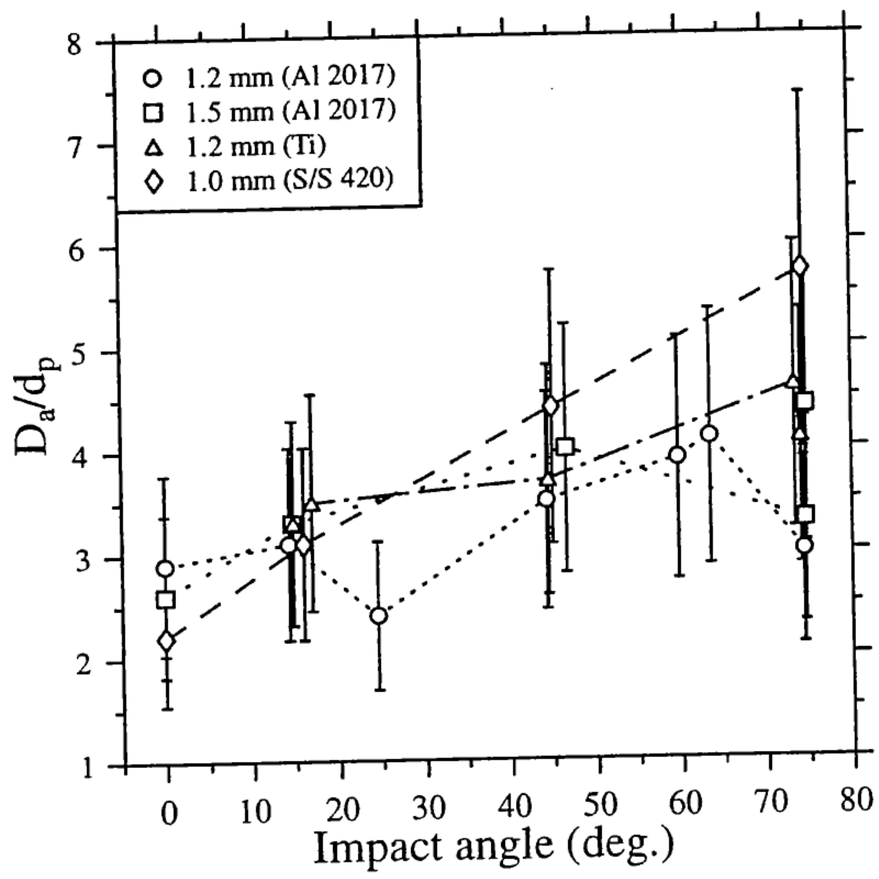

Figure 3. D_a/d_p as a function of projectile density

3.3 Honeycomb damage (X-ray)

Three types of honeycomb cell damage were observed (cell bulged, burst and blasted, where (i) bulged: honeycomb cell deformation, (ii) burst: visible perforation (iii) blast: Al wall removal). The projectile diameter, density and impact angle dependence of the damage is shown in Figs. 4 and 5. The increase in damage is a strong function of projectile density and diameter. Figs. 4 and 5 represent variations in the X-ray opacity of the target :

1. Opaque. Indicative of crumpled / crushed multi-cell walls preventing the transmission of X-rays.
2. Partially transparent. Indicative of foreshortened cells whose walls have been subjected to buckling permitting partial transmission of X-rays.
3. Transparent. Identifies the extent of the entry and/or exit holes.

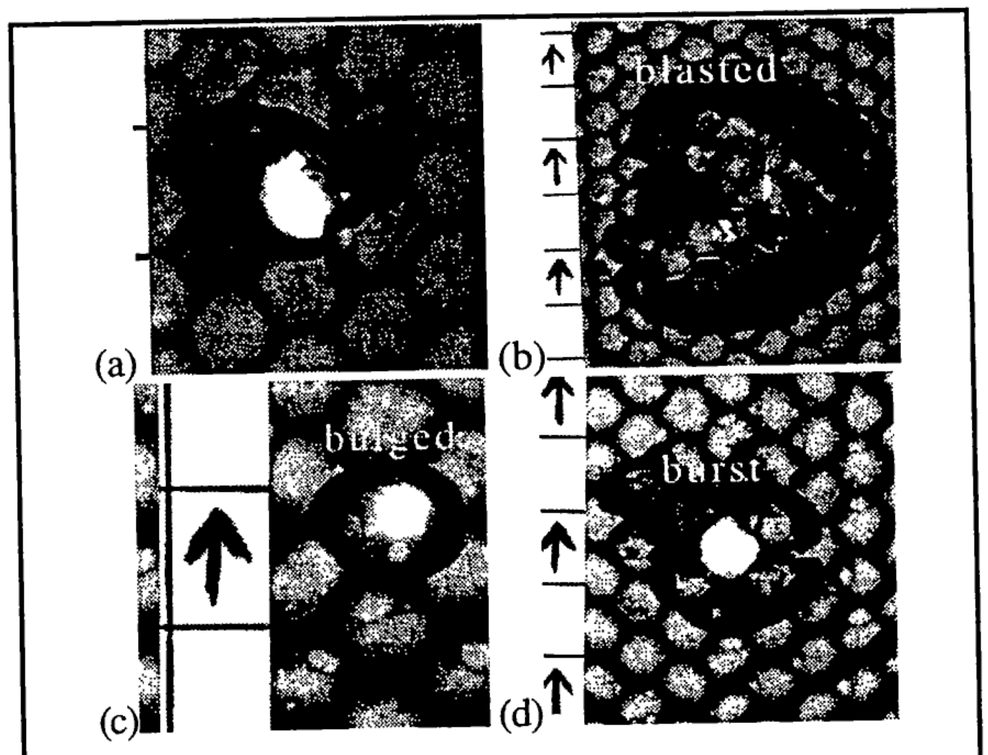

Figure 4. Honeycomb damage. Scale is in cm.
(a,b)1.0 and 2.0 mm Ph. Br. (6.2, 4.8 km s^{-1})
(c,d)1.0 and 2.0 mm Al 2017(5.4, 5.1 km s^{-1})

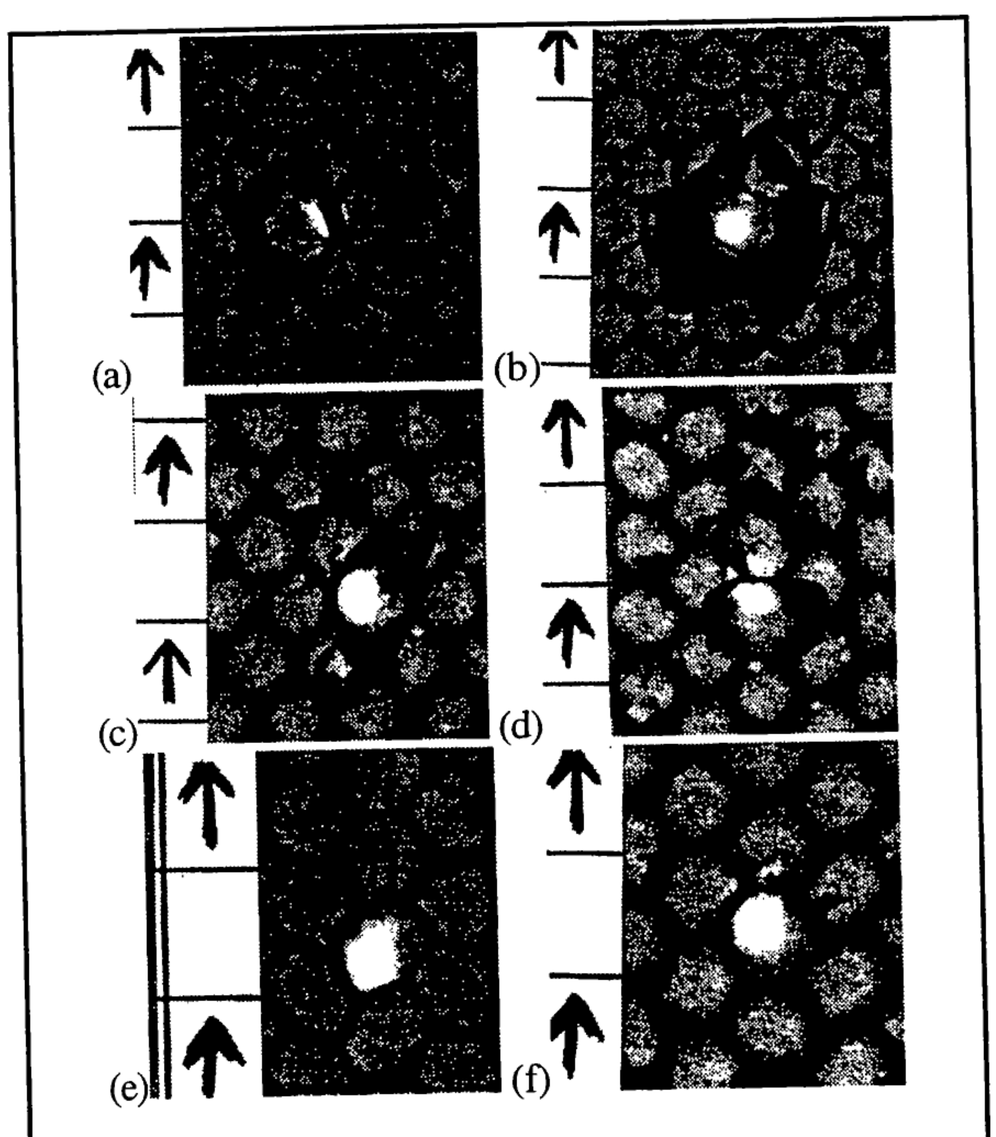

Figure 5. Honeycomb damage for oblique impacts.
(a-c) 1.2 mm Ti. 15°, 45°, 73°(5.0-5.1 km s^{-1})
(d-f) 1.0 mm S/S420. 16°, 45°, 74°(5.1-5.8 km s^{-1})
Scale is in cm. Arrow defines impact direction

The honeycomb damage trends with impact angle and impact energy are given in Figs. 6 and 7. The damage area can be two orders of magnitude greater than the

projectile cross-section. The scattered points in Fig. 6 below the main trend are due to highly oblique impacts. The steep tail-off in damage area at highly oblique impact angles, as shown in Fig. 7, is due to projectile ricochet.

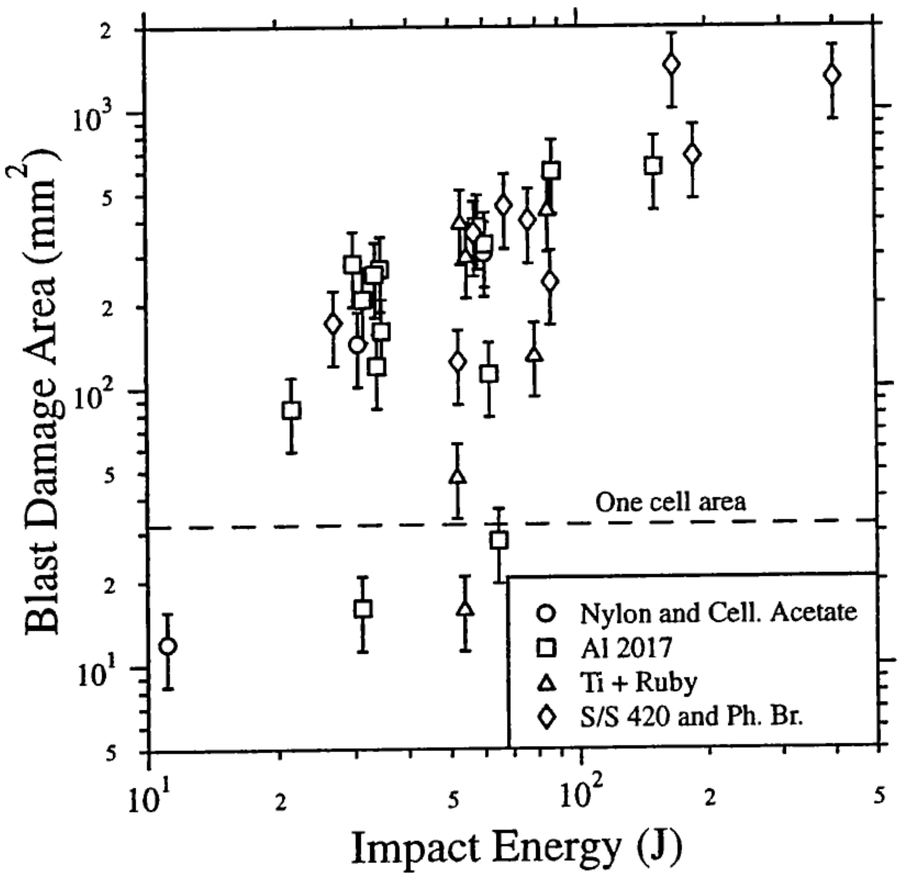

Figure 6. Honeycomb damage as a function of impact energy

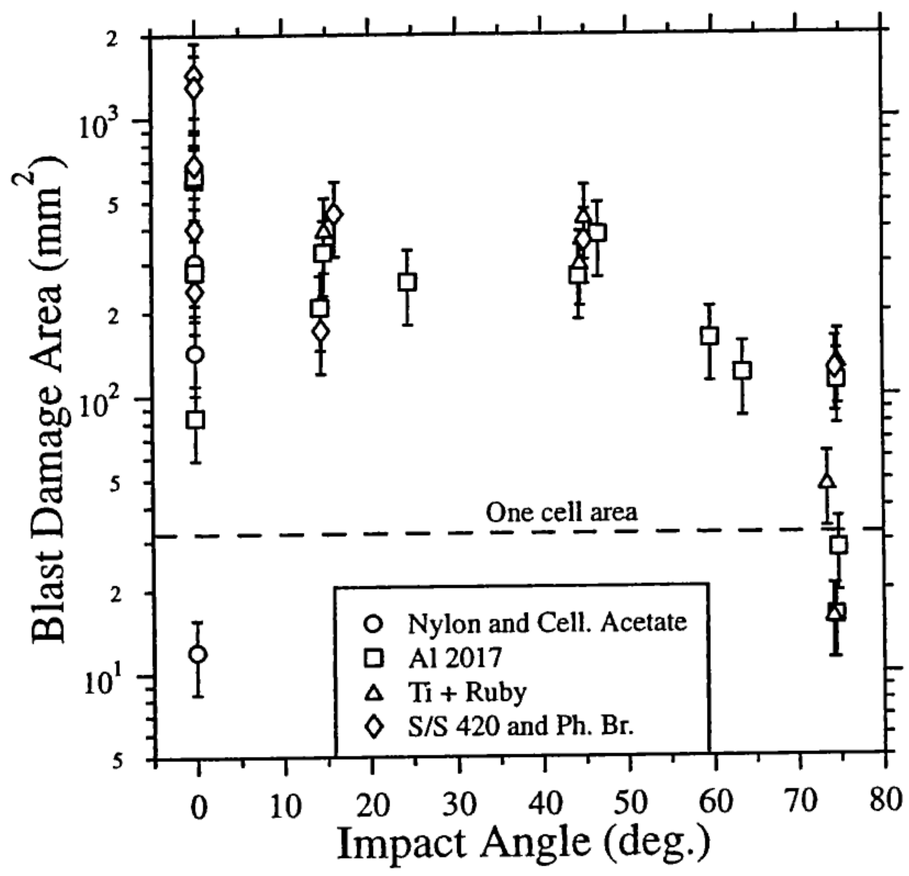

Figure 7. Honeycomb damage as a function of impact angle

3.4 Ballistic limit

Of the 13 normal incidence shots, all the projectiles with a density > 4.5 g cm^{-3} and Al 2017 projectiles with $d_p > 1.2$ mm were found to perforate the rear target (Ref. 2). Only two projectiles from the oblique series of shots presented here exceeded the ballistic limit. (At 15°, the ballistic limit is in the range $1.2 < d_p < 1.5$ mm for Al projectiles and $d_p > 1$ mm for S/S 420 projectiles). The honeycomb is effective at improving the hypervelocity impact shielding performance for oblique impacts.

For normal impacts at a given energy, penetration is determined by projectile density (Ref. 2). The results from this shot programme are plotted in Fig. 8 with the data from Ref. 3. It is noted that only perforating impacts are recorded over 100 J of impactor energy. However, the dependence of impact angle on the ballistic limit can only be assessed for impacts below 100 J.

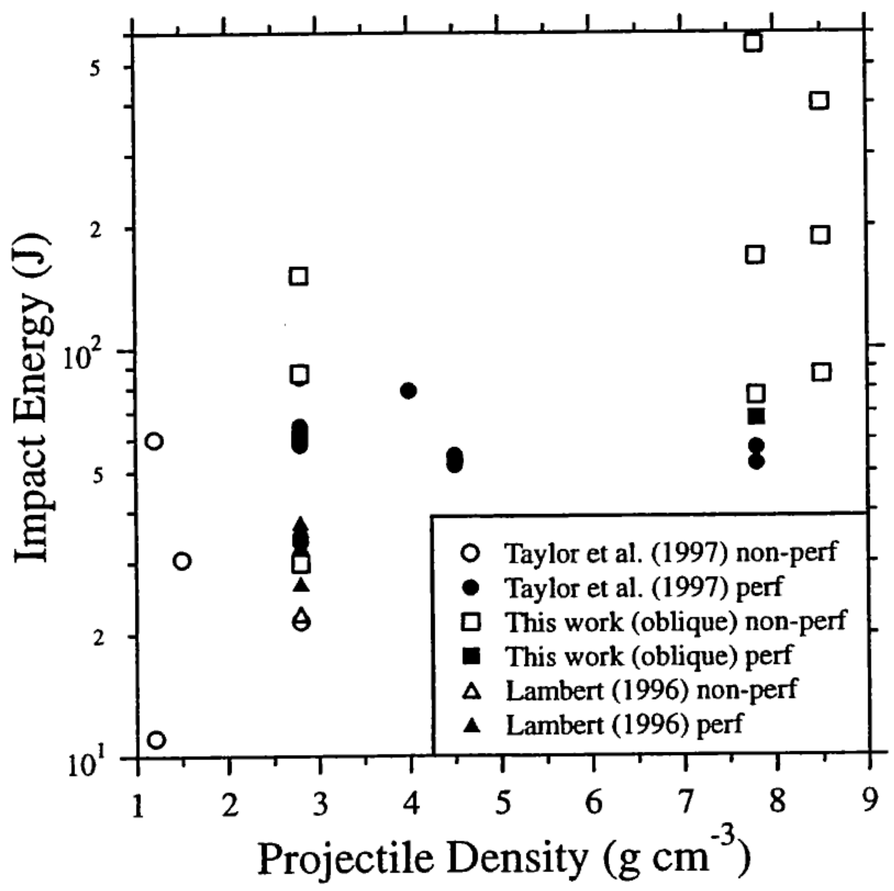

Figure 8. The dependence of ballistic limit on particle density and impact energy

4. DISCUSSION

4.1 Damage equations for CFRP/Al-HC

The simplest form of damage equation is one based on the ballistic limit. In section 3.4, we show that the response is not only a function of the projectile impact energy, but may be enhanced by the impactor density. Further studies to determine the ballistic limit dependence will require tests over a range of impact velocities.

The most applicable form for a damage equation (e.g. in ESABASE DEBRIS) is one based on dual-wall ductile targets. The possibility of an equivalence between CFRP/Al-HC and spaced aluminium plates has previously been suggested, although only in the most general terms (Ref. 5). However, the differing hole growth in composites noted in Ref. 2 suggests that such a comparison may not be possible.

An alternative form of damage equation may be in several parts, where the front hole size may be used to predict the rear hole size, say, and thus the volume of ejecta. In section 3.2, the dependence of D_a/d_p and D_a/D_b are investigated as a function of projectile density and impact angle respectively. The target response variability (plotted as error bars) results in a wide range of potential curve fits. The impact angle term may not follow the $(\cos\theta)^{\alpha}$ used for most damage equations due to the perturbing effect of the honeycomb.

The data presented in Fig. 6 suggest that a damage equation could be developed but would predict only a range of honeycomb damage areas. For $\theta > 70\text{-}75°$, a different relationship will have to be developed (Fig. 7).

We investigate further the form of a potential damage equation by considering impacts onto truss tubes (Ref. 6). Equation 2 was derived from an empirical fit to data. We can define the total area A_h as given by equation 3. The total equivalent hole diameter ($D_{eq(total)}$) is then calculated using equations 1 and 3. This is shown in Fig. 8, plotted against $\sqrt[3]{E}$ for normal (Ref. 2) and oblique impacts, and a relationship can be seen in accordance with the predictions of equation 2.

$$D_{eq\ (total)} \propto E^{1/3} \qquad (2)$$

$$A_h = A_{h\ (front)} + A_{h\ (rear)} \qquad (3)$$

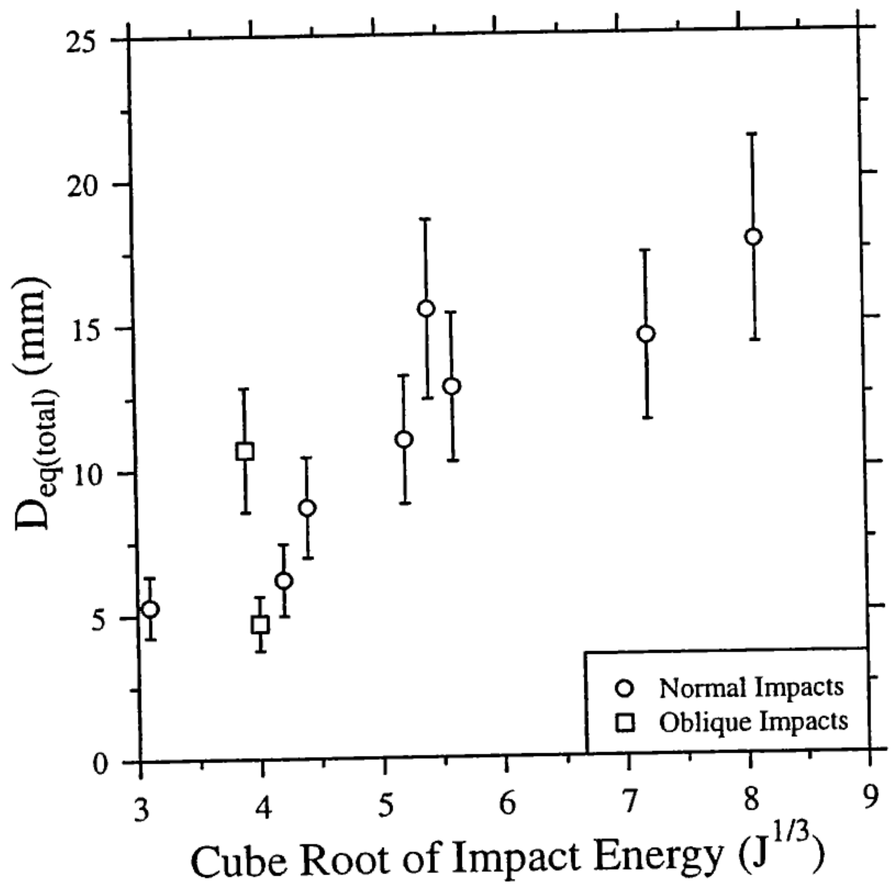

Figure 9. Total hole size as a function of impact energy

This equation can be applied to spaced composite plates and thus to the honeycomb targets used in this work, although the channelling effect of the honeycomb (Ref. 1) may limit the scope of this comparison. In Fig. 9, a linear relationship is suggested for perforating impacts of impact energies below 210 J. This result is similar to that derived from impacts onto truss tubes, where a bimodal fit to the data was also noted (Ref. 6). There is no similar fit for $D_{eq(front)}$ (not shown here).

4.2 Spacecraft subsystems: design considerations

Three types of damage were observed on the target material (Ref. 2):

1. Primary damage (point of particle impact, usually marked by a hole which is often delaminated around the periphery)
2. Secondary damage (resulting from either primary damage or the secondary effects of the impactor(s) passage through the structure- honeycomb damage).
3. Tertiary damage (ejecta damage or freely suspended particles/contaminants resulting from primary and secondary damage. Observed on witness plates and from post-impact handling of the targets).

Primary damage:

1. Propulsion. Tanks usually shrouded behind a second CFRP/Al-HC wall, therefore a penetrative strike with projectile remaining intact (high density projectile, d_p = 2 mm at 5 km s^{-1}) will not cause failure. However, the pipework is less well shielded.
2. EMC. A penetrative hole above a critical size (typically > 5 mm) may reduce EMC. May induce equipment performance degradation over spacecraft lifetime.
3. Thermal. No significant implications result.
4. Structure. Impacts are not likely to compromise the structural integrity in orbit.

Secondary damage :

1. Structure. The damage to the HC core is unlikely to pose significant structural implications on-orbit. However, if the localised honeycomb damage is severe, distortion stresses initiated by thermal cycling effects over an orbital period may give rise to pointing inaccuracies for critical instrumentation.
2. Thermal. The honeycomb damage void potentially reduces the efficiency of the conductive heat flow path if the damage area is large enough.

Tertiary damage :

A large number of contaminants are produced by hypervelocity impact. Non-vaporised debris could enter internal compartments or become ejected from the spacecraft. Internal contamination could potentially disrupt operation of unshielded electronics or harness. External contamination could result in suspended particulates around the spacecraft which may affect exposed optical surfaces and unshielded mechanisms.

5. CONCLUSIONS

The results of a shot programme onto CFRP/Al-HC at 4.5 - 6.2 km s^{-1} using 1.0 - 2.0 mm projectiles over a wide range of densities (1 - 8 g cm^{-3}) are presented. The honeycomb increases the ballistic limit of the target for oblique impacts > 15°. The honeycomb damage area (cell bulge, burst and blast) is significantly larger than the projectile cross-section and is a function of impact energy. For highly oblique impacts, projectile ricochet occurs and the honeycomb cell damage is negligible. The development of a damage equation may be rendered difficult by the target repeatability under hypervelocity impact and will probably require several equations to predict the damage. The greatest risk to spacecraft operations will probably result from the significant ejecta production, both inside and outside the spacecraft.

6. FURTHER WORK

The test data will be compared to dual wall aluminium damage equations. Tests are required at velocities greater than 5 km s^{-1} to determine the velocity dependence.

7. ACKNOWLEDGEMENTS

Thanks are due to Dr. J. Hodgkinson of the Centre for Composite Materials at Imperial College London for providing the X-ray test facility. E. A. Taylor would like to acknowledge financial support from MMS (UK), The Royal Academy of Engineering and the Royal Aeronautical Society.

8. REFERENCES

1. Gehring, J.W. (1970), Chapter IX : Engineering considerations, in *High Velocity Impact Phenomena*, Academic Press, New York, ed. R. Kinslow.
2. Taylor, E.A., Herbert, M.K., Gardner, D.J., Griffiths, A.D., Kay, L., Thomson, R. and Burchell, M.J., Hypervelocity Impact on Carbon Fibre Reinforced Plastic (CFRP) / Aluminium Honeycomb: Risk Assessment for Low Earth Orbiting Spacecraft, Submitted to *Proceedings of the Institution of Mechanical Engineers Part G : Journal of Aerospace Engineering*.
3. Lambert, M. (1996), Hypervelocity impacts and damage laws, presented at COSPAR '96, Birmingham, 14-21 July 1996. Accepted for publication in *Adv. Space Res.*
4. Christiansen, E.L. (1992), Performance equations for advanced orbital debris shields, AIAA 92-1462, presented at the *AIAA Space Programs and Technologies Conference*, March 24-27 1992, Huntsville, AL.
5. Drolshagen, G. and Borde, J. (1992), *ESABASE Debris-Meteoroid/Debris Impact Analysis Technical Description*, ESA ESTEC, ESABASE-GD-01/1, Noordwijk, Netherlands.
6. Christiansen, E.L. (1990), Investigation of hypervelocity impact damage to space station truss tubes, *Int. J. Impact Engng.*, Vol. 10, pp. 125-133.
7. Terrillon, F., Warren, H.R. and Yelle, M.J. (1991), Orbital debris shielding design of the Radarsat spacecraft, IAF-91-283, *42nd International Astronautical Congress*, 5-11 October 1991, Montreal, Canada.

APPENDIX 1

Author	No	Target	d_p(mm)	proj. type	v (km s^{-1})	θ(°)	d_p/f	Comments
Taylor et al. (this work)	21	CFRP/Al-HC	0.8-1.5	Table 2	4.7-5.8	15-75	0.5-1.0	This paper.
Taylor et al. (Ref. 2)	15	CFRP/Al-HC	0.8-2.0	Table 2	4.5-6.2	0	0.5-1.25	Ballistic limit is a function of projectile density.
Lambert (1996) (Ref. 3)	3 4 3 2	CFRP plate CFRP plate+MLI CFRP/Al-HC CFRP/Al-HC+MLI	0.7-1.2 0.9-1.2 0.9-1.1 1.1-1.5	Al	6.0-6.2 5.8-6.6 5.3-6.6 6.4-6.5	0	0.2-0.3 - 0.8-1.0 -	MLI increases the ballistic limit by a factor of 3.
Terrillon et al. (1992) (Ref. 7)	2 2 1	Al-HC Al-HC Composite HC	1.0 1.0 1.0	Al	6.9-7.5 7.4-8.1 -	20,70 20,70 70	2.44 1.96 -	Rear hole is on-axis with entry hole, suggesting channelling.
Christiansen (1990)(Ref. 6)	58	Tubes	0.6 - 3.2	glass Al	3.3-7.8	0, 45	0.31 - 1.77	$D_{eq(total)} \propto E^{1/3}$.
Gehring (1970)(Ref. 1)	14	Cd/Al-HC	3.18	Cd	6.5-7.0	0	2.0-9.6	Channelling effect of honeycomb identified.

Table A1. Summary of hypervelocity impact studies pertinent to this work.